PERGAMON

International Journal of Solids and Structures 39 (2002) 6081–6102

INTERNATIONAL JOURNAL OF SOLIDS and STRUCTURES

www.elsevier.com/locate/ijsolstr

# Exact vibration solutions for circular Mindlin plates with multiple concentric ring supports

Y. Xiang *

*School of Engineering and Industrial Design, Centre for Construction Technology and Research, University of Western Sydney, Building X, Kingswood Campus Locked Bag, Penrith South DC, NSW 1797, Australia*

Received 30 April 2002; received in revised form 7 August 2002

**Abstract**

This paper presents an analytical approach to investigate the vibration behaviour of circular Mindlin plates with multiple concentric ring supports. A circular plate is first divided into multiple annular segments and a circular segment at the locations of the ring supports. The governing differential equations and the solutions of these equations for the annular and circular segments based on the Mindlin plate theory are presented. A homogenous equation system governing the vibration of circular Mindlin plates with ring supports is derived by imposing the essential and natural boundary and segment interface conditions. The first known exact vibration frequencies for circular Mindlin plates with multiple concentric ring supports are obtained and the modal shapes of displacement fields and stress resultants for several selected cases are presented. The influence of the ring support locations, plate boundary conditions and plate thickness ratios on the vibration behaviour of circular plates is discussed.


*Keywords:* Circular Mindlin plates; Concentric ring supports; Domain decomposition technique; Exact solutions; Vibration

## 1. Introduction

Circular plates are important structural components that are widely used in civil, mechanical, aerospace, marine and computer engineering. There are literally hundreds of papers in open literature on free vibration of circular plates which have been well documented in the excellent reviews of Leissa (1969, 1977a,b, 1981a,b, 1987a,b) and other publications (i.e. Liew, 1994; McGee et al., 1995; Laura et al., 1996; Liew et al., 1995, 1997; Liew and Yang, 1999, 2000; Chakraverty and Petyt, 1999; Elishakoff, 2000; Wu and Liu, 2001).

Most of the studies on vibration of circular plates are based on the Kirchhoff thin plate theory. It is well known that the effect of transverse shear deformation and rotary inertia is neglected in the thin plate theory

* Tel.: +61-2-4736-0395; fax: +61-2-4736-0833.
*E-mail address:* y.xiang@uws.edu.au (Y. Xiang).

0020-7683/02/$ - see front matter 
PII: S0020-7683(02)00494-8

that leads to overestimation of the vibration frequencies when a plate becomes moderately thick. Several first order and higher order thick plate theories have been proposed in the past five decades to account for the effect of transverse shear deformation and rotary inertia (i.e. Reissner, 1945; Mindlin, 1951; Levinson, 1980; Reddy, 1984; Leung, 1991). Among these theories, the Mindlin first order shear deformable plate theory (Mindlin, 1951) has been widely accepted by researchers to study vibration of moderately thick circular plates (Mindlin and Deresiewicz, 1954; Rao and Prasad, 1980; Irie et al., 1982; Gupta and Lal, 1985; Aksu and Al-Kaabi, 1987; Liew et al., 1993, 1994, 1997, 1998).

Vibration of circular plates with concentric ring supports has been investigated by many researchers (i.e. Bodine, 1959; Kunukkasseril and Swamidas, 1974; Singh and Mirza, 1976; Narita, 1983; Laura et al., 1987; Kim and Dickinson, 1989; Lam and Liew, 1992; Liew and Lam, 1993; Wang and Thevendran, 1993; Liew et al., 1993, 1994; Chou et al., 1999; Wang, 2001). All these studies are based on the thin plate theory except the ones by Liew et al. (1993, 1994) and Chou et al. (1999). Employing the p-Ritz method, Liew et al. (1993, 1994) studied vibration of circular and annular Mindlin plates with one and two concentric ring supports. Extensive vibration frequencies for circular and annular Mindlin plates with ring supports were documented (Liew et al., 1993, 1994). Chou et al. (1999) studied the optimal locations of ring and elastic ring supports to maximize the axisymmetric vibration frequencies of circular Mindlin plates. The Rayleigh–Ritz method and the analytical method were employed in their study to obtain the vibration frequencies and nodal lines of the plates.

To the author's best knowledge, there is virtually no exact solution available in open literature for vibration of circular Mindlin plates with concentric ring supports. This paper aims to fill the apparent gap in this area by developing an analytical approach for vibration analysis of circular Mindlin plates with multiple concentric ring supports and by presenting exact vibration solutions for such plates. Employing the domain decomposition technique, a circular plate is decomposed to multiple annular segments and a circular segment at the locations of the ring supports. Based on the Mindlin plate theory, the governing equations of motion and the general solutions of these equations for the annular and circular segments are derived. The essential and natural boundary conditions and segment interface conditions are imposed and a homogenous equation system that governs the vibration of circular Mindlin plates with ring supports is derived. A comparison study is carried out to verify the correctness of the proposed method. Extensive exact solutions for vibration of circular Mindlin plates with one, two and three ring supports are presented in tabular and graphical forms. The modal shapes of displacement fields and stress resultants are presented for several selected cases. The exact vibration solutions presented in this paper is extremely important as benchmark values for researchers to check their numerical models and for engineers to design such plate structures.

## 2. Mathematical modelling

Consider an isotropic, flat circular plate of radius $R$, thickness $h$, mass density $\rho$, Poisson's ratio $v$, Young's modulus $E$ and shear modulus $G\ (= E/[2(1+v)])$. The plate may have free, simply supported or clamped edge support conditions and $m$ concentric ring supports with radii $a_1, a_2, \ldots, a_m$, as shown in Fig. 1. The rings impose zero deflection constraint along the ring supports in the plate. The problem at hand is to determine the exact vibration frequencies of the ring supported circular plates.

The plate is first divided into $m$ annular segments plus one circular segment at the locations of the concentric ring supports (see Fig. 1). The Mindlin first order shear deformable plate theory (Mindlin, 1951) is employed in this study. Using the polar coordinate system (see Fig. 1), the equations of motion for the $i$th segment in harmonic vibration may be derived as (Mindlin and Deresiewicz, 1954):

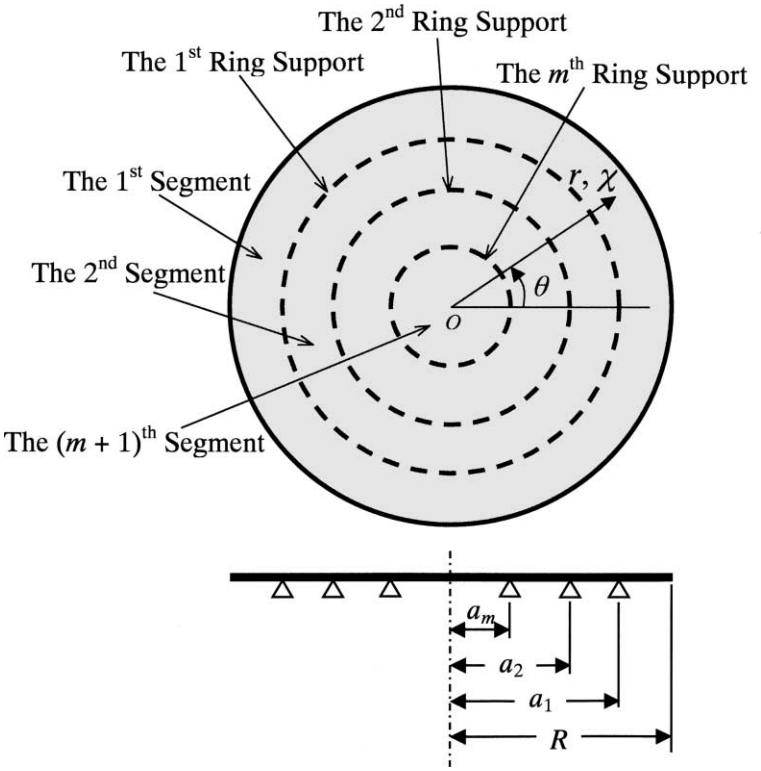


Fig. 1. Geometry and coordinate system for a circular plate with multiple concentric ring supports.

$$\frac{\partial}{\partial r}\left\{D\left[\frac{\partial\psi_r^i}{\partial r}+\frac{\nu}{r}\left(\psi_r^i+\frac{\partial\psi_\theta^i}{\partial\theta}\right)\right]\right\}+\frac{1}{r}\frac{\partial}{\partial\theta}\left\{\frac{(1-\nu)D}{2}\left[\frac{1}{r}\left(\frac{\partial\psi_r^i}{\partial\theta}-\psi_\theta^i\right)+\frac{\partial\psi_\theta^i}{\partial r}\right]\right\}$$
$$+\frac{1}{r}\left\{D\left[\frac{\partial\psi_r^i}{\partial r}+\frac{\nu}{r}\left(\psi_r^i+\frac{\partial\psi_\theta^i}{\partial\theta}\right)\right]-D\left[\frac{1}{r}\left(\psi_r^i+\frac{\partial\psi_\theta^i}{\partial\theta}\right)+\nu\frac{\partial\psi_r^i}{\partial r}\right]\right\}-\kappa^2Gh\left(\psi_r^i+\frac{\partial w^i}{\partial r}\right)+\frac{\rho h^3\omega^2}{12}\psi_r^i=0 \tag{1}$$

$$\frac{\partial}{\partial r}\left\{\frac{(1-\nu)D}{2}\left[\frac{1}{r}\left(\frac{\partial\psi_r^i}{\partial\theta}-\psi_\theta^i\right)+\frac{\partial\psi_\theta^i}{\partial r}\right]\right\}+\frac{1}{r}\frac{\partial}{\partial\theta}\left\{D\left[\frac{1}{r}\left(\psi_r^i+\frac{\partial\psi_\theta^i}{\partial\theta}\right)+\nu\frac{\partial\psi_r^i}{\partial r}\right]\right\}$$
$$+\frac{2}{r}\left\{\frac{(1-\nu)D}{2}\left[\frac{1}{r}\left(\frac{\partial\psi_r^i}{\partial\theta}-\psi_\theta^i\right)+\frac{\partial\psi_\theta^i}{\partial r}\right]\right\}-\kappa^2Gh\left(\psi_\theta^i+\frac{1}{r}\frac{\partial w^i}{\partial\theta}\right)+\frac{\rho h^3\omega^2}{12}\psi_\theta^i=0 \tag{2}$$

$$\frac{1}{r}\left[\kappa^2Gh\left(\psi_r^i+\frac{\partial w^i}{\partial r}\right)\right]+\frac{\partial}{\partial r}\left[\kappa^2Gh\left(\psi_r^i+\frac{\partial w^i}{\partial r}\right)\right]+\frac{1}{r}\frac{\partial}{\partial\theta}\left[\kappa^2Gh\left(\psi_\theta^i+\frac{1}{r}\frac{\partial w^i}{\partial\theta}\right)\right]+\rho h\omega^2w^i=0 \tag{3}$$

in which $w^i$, $\psi_r^i$ and $\psi_\theta^i$ are the transverse deflection and the rotations in the $\theta$ and $r$ directions at the midsurface of the plate, respectively, $r$ and $\theta$ are the radial and the circumferential coordinates, $D$ $(= Eh^3/[12(1-\nu^2)])$ is the flexural rigidity of the plate, $\kappa^2$ is the shear correction factor required in the Mindlin plate theory, and $\omega$ is the circular frequency.

Mindlin and Deresiewicz (1954) proposed that the displacement fields of the plate may be expressed as functions of three potentials $\Theta_1^i$, $\Theta_2^i$ and $\Theta_3^i$:

$$\psi_r^i = (\sigma_1 - 1)\frac{\partial \Theta_1^i}{\partial \chi} + (\sigma_2 - 1)\frac{\partial \Theta_2^i}{\partial \chi} + \frac{1}{\chi}\frac{\partial \Theta_3^i}{\partial \theta} \tag{4}$$

$$\psi_\theta^i = (\sigma_1 - 1)\frac{1}{\chi}\frac{\partial \Theta_1^i}{\partial \theta} + (\sigma_2 - 1)\frac{1}{\chi}\frac{\partial \Theta_2^i}{\partial \theta} - \frac{\partial \Theta_3^i}{\partial \chi} \tag{5}$$

$$\bar{w}^i = \Theta_1^i + \Theta_2^i \tag{6}$$

where

$$\sigma_1, \sigma_2 = \frac{(\delta_2^2, \delta_1^2)}{\left[\dfrac{\tau^2\lambda^2}{12} - \dfrac{6(1-v)\kappa^2}{\tau^2}\right]} = \frac{2(\delta_2^2, \delta_1^2)}{\delta_3^2(1-v)} \tag{7}$$

$$\delta_1^2, \delta_2^2 = \frac{\lambda^2}{2}\left[\frac{\tau^2}{12} + \frac{\tau^2}{6(1-v)\kappa^2} \pm \sqrt{\left(\frac{\tau^2}{12} - \frac{\tau^2}{6(1-v)\kappa^2}\right)^2 + \frac{4}{\lambda^2}}\right] \tag{8}$$

$$\delta_3^2 = \frac{2}{(1-v)}\left[\frac{\tau^2\lambda^2}{12} - \frac{6(1-v)\kappa^2}{\tau^2}\right] \tag{9}$$

$$\bar{w}^i = \frac{w^i}{R}, \quad \chi = \frac{r}{R}, \quad \tau = \frac{h}{R}, \quad \lambda = \omega R^2\sqrt{\frac{\rho h}{D}} \tag{10}$$

in which $\bar{w}^i$ is the non-dimensionalised deflection of the plate, $\chi$ is the non-dimensionalised radial coordinate (see Fig. 1), and $\lambda$ is the frequency parameter.

Based on the three potentials, the governing differential equations of the vibrating annular or circular segment, in polar coordinates, may be derived as

$$(\nabla^2 + \delta_1^2)\Theta_1^i = 0 \tag{11}$$

$$(\nabla^2 + \delta_2^2)\Theta_2^i = 0 \tag{12}$$

$$(\nabla^2 + \delta_3^2)\Theta_3^i = 0 \tag{13}$$

where the Laplacian operator

$$\nabla^2(\bullet) = \frac{\partial^2(\bullet)}{\partial \chi^2} + \frac{1}{\chi}\frac{\partial(\bullet)}{\partial \chi} + \frac{1}{\chi^2}\frac{\partial^2(\bullet)}{\partial \theta^2} \tag{14}$$

The solutions to Eqs. (11)–(13) for the annular segment ($i = 1, 2, \ldots, m$) and the circular segment ($i = m + 1$) are

$$\Theta_1^i = A_1^i R_n^i(\Delta_1\chi)\cos n\theta + B_1^i S_n^i(\Delta_1\chi)\cos n\theta \tag{15}$$

$$\Theta_2^i = A_2^i R_n^i(\Delta_2\chi)\cos n\theta + B_2^i S_n^i(\Delta_2\chi)\cos n\theta \tag{16}$$

$$\Theta_3^i = A_3^i R_n^i(\Delta_3\chi)\sin n\theta + B_3^i S_n^i(\Delta_3\chi)\sin n\theta \tag{17}$$

where

$$\Delta_j = \begin{cases} \delta_j & \text{if } \delta_j^2 \geqslant 0 \\ \mathrm{Im}(\delta_j) & \text{if } \delta_j^2 < 0 \end{cases} \quad j = 1,2,3 \tag{18}$$

$$R_n^i(\Delta_j\chi) = \begin{cases} J_n(\Delta_j\chi) & \text{if } \delta_j^2 \geqslant 0 \\ I_n(\Delta_j\chi) & \text{if } \delta_j^2 < 0 \end{cases} \quad j = 1,2,3 \tag{19}$$

$$S_n^i(\Delta_j\chi) = \begin{cases} Y_n(\Delta_j\chi) & \text{if } \delta_j^2 \geqslant 0 \\ K_n(\Delta_j\chi) & \text{if } \delta_j^2 < 0 \end{cases} \quad j = 1,2,3 \tag{20}$$

in which $A_j^i$ and $B_j^i$, $j = 1$, 2 and 3, are the arbitrary constants that will be determined by the plate boundary conditions and interface continuity conditions between segments, $n$ is the number of nodal diameters of a vibration mode, $J_n(\bullet)$ and $I_n(\bullet)$ are the first kind and the modified first kind Bessel functions of order $n$, respectively, and $Y_n(\bullet)$ and $K_n(\bullet)$ are the second kind and the modified second kind Bessel functions of order $n$, respectively. Note that for the circular segment $(i = m + 1)$, the arbitrary constants $B_j^i$ must be set to zero to prevent singularity for the displacement fields $w^i$, $\psi_r^i$ and $\psi_\theta^i$ at the plate centre $(\chi = r/R = 0)$.

The periphery conditions of circular Mindlin plates at the edge ($i = 1$ and $\chi = r/R = 1$) are given by the boundary conditions defined in Eqs. (21)–(23):

$$M_{rr}^i = M_{r\theta}^i = Q_r^i = 0, \text{ for free edge} \tag{21}$$

$$M_{rr}^i = \psi_\theta^i = \bar{w}^i = 0, \text{ for simply supported edge} \tag{22}$$

$$\psi_r^i = \psi_\theta^i = \bar{w}^i = 0, \text{ for clamped edge} \tag{23}$$

where the stress resultants for shear force and bending moment $Q_r^i$, $M_{rr}^i$ and $M_{r\theta}^i$ are given by (Liew et al., 1998)

$$Q_r^i = \kappa^2 Gh\left(\frac{\partial \bar{w}^i}{\partial \chi} + \psi_r^i\right) \tag{24}$$

$$M_{rr}^i = \frac{D}{R}\left[\frac{\partial \psi_r^i}{\partial \chi} + \frac{v}{\chi}\left(\psi_r^i + \frac{\partial \psi_\theta^i}{\partial \theta}\right)\right] \tag{25}$$

$$M_{r\theta}^i = \frac{D}{R}\left(\frac{1-v}{2}\right)\left[\frac{1}{\chi}\left(\frac{\partial \psi_r^i}{\partial \theta} - \psi_\theta^i\right) + \frac{\partial \psi_\theta^i}{\partial \chi}\right] \tag{26}$$

To satisfy the ring support conditions and to ensure the continuity along the interface of the $i$th and the $(i+1)$th segments, the essential and natural interface conditions between the two segments must hold as follows:

$$\bar{w}^i = 0 \tag{27}$$

$$\bar{w}^{i+1} = 0 \tag{28}$$

$$\psi_r^i = \psi_r^{i+1} \tag{29}$$

$$\psi_\theta^i = \psi_\theta^{i+1} \tag{30}$$

$$M_{rr}^{i} = M_{rr}^{i+1} \tag{31}$$

$$M_{r\theta}^{i} = M_{r\theta}^{i+1} \tag{32}$$

The displacement fields and the stress resultants of the $i$th segment may be expressed in terms of the arbitrary constants $A_j^i$ and $B_j^i$, $j = 1$, 2 and 3, as given in Appendix A. In view of Eqs. (4)–(6) and (15)–(17), a homogeneous system of equations can be derived by implementing the boundary conditions of the plate along the circular edge (Eqs. (21)–(23)) and the interface conditions between two segments (Eqs. (27)–(32)) when assembling the segments to form the entire circular plate

$$\mathbf{K}\begin{Bmatrix} \mathbf{A}^1 \\ \mathbf{B}^1 \\ \vdots \\ \mathbf{A}^i \\ \mathbf{B}^i \\ \vdots \\ \mathbf{A}^m \\ \mathbf{B}^m \\ \mathbf{A}^{m+1} \end{Bmatrix} = \{\mathbf{0}\} \tag{33}$$

where

$$\mathbf{A}^i = \begin{Bmatrix} A_1^i \\ A_2^i \\ A_3^i \end{Bmatrix}, \quad \mathbf{B}^i = \begin{Bmatrix} B_1^i \\ B_2^i \\ B_3^i \end{Bmatrix} \tag{34}$$

and $\mathbf{K}$ is a $[6(m+1)-3] \times [6(m+1)-3]$ matrix. The angular frequency $\omega$ of the plate is evaluated by setting the determinant of $\mathbf{K}$ in Eq. (33) to be zero.

## 3. Results and discussion

The proposed analytical method may be employed to obtain exact vibration frequencies for circular Mindlin plates with arbitrary number of concentric ring supports. The vibration solutions presented in this paper are limited to circular plates with one, two, and three concentric ring supports. The vibration frequency $\omega$ is expressed in terms of a non-dimensionalised frequency parameter $\lambda = \omega R^2\sqrt{\rho h/D}$. The Poisson's ratio $\nu = 0.3$ and the shear correction factor $\kappa^2 = 5/6$ are adopted in all calculations in this paper.

### 3.1. Verification of solution approach

Table 1 presents the frequency parameters $\lambda$ generated by the present solution approach and the p-Ritz method (Liew et al., 1993) for circular Mindlin plates with one concentric ring support ($h/R = 0.10, a_1/R = 0.5$). It is seen that the exact vibration solutions from the proposed analytical approach are in good agreement with the results from the p-Ritz method (Liew et al., 1993). The results in Table 1 show that the p-Ritz solutions (Liew et al., 1993) have not converged to the exact solutions yet. The comparison study confirms the correctness of the analytical method used in this paper.

Table 1
Comparison study for frequency parameters $\lambda = \omega R^2\sqrt{\rho h/D}$ of circular Mindlin plates with one concentric ring support ($h/R = 0.10$, $a_1/R = 0.5$)

| Boundary conditions | Sources | Mode sequence | | | | | |
|---|---|---|---|---|---|---|---|
| | | 1 | 2 | 3 | 4 | 5 | 6 |
| Free | Liew et al. (1993) | 6.843 | 8.931 | 11.142 | 15.566 | 22.749 | 29.412 |
| | Present | 6.83928 | 8.90416 | 11.0688 | 15.4546 | 22.6299 | 29.2910 |
| Simply supported | Liew et al. (1993) | 26.386 | 41.909 | 47.026 | 48.599 | 55.859 | 65.204 |
| | Present | 26.3530 | 41.7900 | 46.4633 | 48.1824 | 55.2252 | 64.4400 |
| Clamped | Liew et al. (1993) | 28.492 | 53.868 | 63.177 | 64.865 | 71.578 | 72.478 |
| | Present | 28.3852 | 53.8662 | 62.5998 | 64.4380 | 70.7750 | 71.0430 |

### 3.2. Circular plates with one concentric ring support

Tables 2–4 present the exact frequency parameters of the first 10 modes for free, simply supported and clamped circular Mindlin plates with one concentric ring support. The plate thickness ratio $h/R$ varies from 0.05 to 0.1 to 0.2 and the ring support location $a_1/R$ is set to be 0.1, 0.5 and 0.9, respectively. The values in bracket $(n, s)$ indicate that the vibrating mode has $n$ nodal diameters and vibrates in the $s$th mode for the given $n$ value. We observe that the fundamental vibration mode is axisymmetric ($n = 0$) for all cases in Tables 2–4 except for free circular plates with ring location at $a_1/R = 0.1$ where a nodal diameter ($n = 1$) exists in the vibration mode. As expected, the frequency parameters $\lambda$ decrease as the plate thickness ratio $h/R$ increases due to the effect of transverse share deformation and rotary inertia in the plate.

The exact results in Tables 2–4 are very valuable as benchmarks for checking approximate numerical solutions. However, these results are not sufficient to reveal the effect of ring supports on the vibration behaviour of circular plates. To complement the results in Tables 2–4, Figs. 2–4 depict the frequency parameters $\lambda$ of the first four modes against the ring support locations $a_1/R$ for free, simply supported and clamped circular Mindlin plates, respectively. Each curve in Figs. 2–4 has 99 sample points and starts at $a_1/R = 0.01$ and ends at $a_1/R = 0.99$.

We observe in Fig. 2 that the frequency parameters $\lambda$ for free circular plates increase first and then decrease when the ring support location parameter $a_1/R$ varies from 0.01 to 0.99. The optimal location of the ring support in maximizing the fundamental frequency parameter is at $a_1/R \approx 0.7$. The optimal locations of the ring support in maximizing frequency parameters of the second, third and fourth modes are at $a_1/R \approx 0.78$, 0.83 and 0.85, respectively. It is noted that the optimal location of the ring support to maximize the fundamental frequency of a circular plate is at the circumferential nodal line corresponding to the higher mode of the circular plate without the ring support, as indicated by Laura (1999) and proved by Chou et al. (1999). Several kink points can be observed on the curves (see Fig. 2). These kind points represent the locations where mode shape switching occurs when the ring support location $a_1/R$ varies across these kink points. We observe that the variations of frequency parameters $\lambda$ versus the ring support location $a_1/R$ show very similar trends for free circular plates with different plate thickness ratios $h/R$. The frequency parameters $\lambda$ decrease as the plate thickness ratio $h/R$ increases due to the effect of transverse shear deformation and rotary inertia in the plates.

The variations of frequency parameters $\lambda$ of the first four modes against the ring support location $a_1/R$ for simply supported circular Mindlin plates are shown in Fig. 3. The frequency parameters $\lambda$ for the first three modes increase first and then decrease as the ring support moves from $a_1/R = 0.01$–$0.99$. The frequency parameter $\lambda$ for the fourth mode shows a slightly different pattern where a local maximum frequency parameter $\lambda$ exists at $a_1/R \approx 0.4$ (see Fig. 2). The optimal ring support locations for the first four modes are at $a_1/R \approx 0.45$, 0.56, 0.62 and 0.65, respectively. Again, we observe kink points on the curves for the third and fourth modes that indicate locations of mode shape switching.

Table 2
Frequency parameters $\lambda = \omega R^2\sqrt{\rho h/D}$ for circular Mindlin plates with one concentric ring support ($h/R = 0.05$)

| Edge conditions | $\frac{a_1}{R}$ | Mode sequence | | | | | | | | | |
|---|---|---|---|---|---|---|---|---|---|---|---|
| | | 1 | 2 | 3 | 4 | 5 | 6 | 7 | 8 | 9 | 10 |
| Free | 0.1 | 3.06587(1,1) | 3.89167(0,1) | 5.46743(2,1) | 12.3152(3,1) | 21.4945(4,1) | 22.6190(0,2) | 25.6563(1,2) | 32.7720(5,1) | 35.4809(2,2) | 46.0419(6,1) |
| | 0.5 | 6.90657(0,1) | 9.14919(1,1) | 11.5712(2,1) | 16.2262(3,1) | 23.7795(4,1) | 30.7854(0,2) | 34.0529(5,1) | 46.7351(6,1) | 58.2173(1,2) | 61.5683(7,1) |
| | 0.9 | 6.21766(0,1) | 17.1719(1,1) | 31.4204(2,1) | 35.6169(0,2) | 48.5801(3,1) | 56.9906(1,2) | 68.3295(4,1) | 80.8041(2,2) | 84.3371(0,3) | 90.3781(5,1) |
| Simply supported | 0.1 | 15.9477(0,1) | 18.0137(1,1) | 25.8983(2,1) | 39.2842(3,1) | 53.6551(0,2) | 55.4289(4,1) | 58.0565(1,2) | 70.3601(2,2) | 73.6967(5,1) | 90.9916(3,2) |
| | 0.5 | 27.4127(0,1) | 44.4313(1,1) | 50.8159(0,2) | 52.3044(2,1) | 60.7225(3,1) | 71.5226(4,1) | 72.8250(1,2) | 85.1760(5,1) | 101.742(6,1) | 113.120(2,2) |
| | 0.9 | 11.5784(0,1) | 24.0420(1,1) | 39.2904(2,1) | 44.7102(0,2) | 57.1881(3,1) | 67.8791(1,2) | 77.5664(4,1) | 93.5655(2,2) | 98.3731(0,3) | 100.256(5,1) |
| Clamped | 0.1 | 24.4093(0,1) | 26.6938(1,1) | 35.0461(2,1) | 49.5938(3,1) | 66.5504(0,2) | 66.9957(4,1) | 71.2613(1,2) | 83.8848(2,2) | 86.3813(5,1) | 105.207(3,2) |
| | 0.5 | 30.0090(0,1) | 58.6722(1,1) | 71.1864(0,2) | 73.1268(2,1) | 81.8158(3,1) | 82.4579(1,2) | 91.8631(4,1) | 104.553(5,1) | 116.664(2,2) | 120.233(6,1) |
| | 0.9 | 11.6224(0,1) | 24.1212(1,1) | 39.4019(2,1) | 44.8387(0,2) | 57.3273(3,1) | 68.0487(1,2) | 77.7276(4,1) | 93.7683(2,2) | 98.5899(0,3) | 100.434(5,1) |

The values in brackets $(n,s)$ denote the number of nodal diameters $(n)$ and the mode sequence $(s)$ for a given $n$ value.

Table 3
Frequency parameters $\lambda = \omega R^2\sqrt{\rho h/D}$ for circular Mindlin plates with one concentric ring support ($h/R = 0.10$)

| Edge conditions | $\frac{a_1}{R}$ | Mode sequence | | | | | | | | | |
|---|---|---|---|---|---|---|---|---|---|---|---|
| | | 1 | 2 | 3 | 4 | 5 | 6 | 7 | 8 | 9 | 10 |
| Free | 0.1 | 2.74403(1,1) | 3.84013(0,1) | 5.35033(2,1) | 12.0680(3,1) | 20.8089(4,1) | 21.4867(0,2) | 23.8181(1,2) | 31.2861(5,1) | 33.5118(2,2) | 43.2853(6,1) |
| | 0.5 | 6.83928(0,1) | 8.90416(1,1) | 11.0688(2,1) | 15.4546(3,1) | 22.6299(4,1) | 29.2910(0,2) | 32.2207(5,1) | 43.7481(6,1) | 54.2911(1,2) | 56.8303(7,1) |
| | 0.9 | 6.16531(0,1) | 16.7548(1,1) | 30.0802(2,1) | 34.0242(0,2) | 45.5681(3,1) | 53.1649(1,2) | 62.7534(4,1) | 73.5866(2,2) | 76.6309(0,3) | 81.2524(5,1) |
| Simply supported | 0.1 | 15.2997(0,1) | 16.8367(1,1) | 24.8167(2,1) | 37.3895(3,1) | 49.3470(0,2) | 51.8441(4,1) | 52.4120(1,2) | 64.0233(2,2) | 67.6448(5,1) | 82.0370(3,2) |
| | 0.5 | 26.3530(0,1) | 41.7900(1,1) | 46.4633(0,2) | 48.1824(2,1) | 55.2252(3,1) | 64.4400(4,1) | 64.8304(1,2) | 76.0655(5,1) | 89.9230(6,1) | 98.2091(2,2) |
| | 0.9 | 10.9665(0,1) | 22.4829(1,1) | 36.1847(2,1) | 40.9852(0,2) | 51.7735(3,1) | 60.9064(1,2) | 68.9463(4,1) | 82.1206(2,2) | 86.0274(0,3) | 87.4331(5,1) |
| Clamped | 0.1 | 22.9636(0,1) | 24.4809(1,1) | 32.6913(2,1) | 45.8446(3,1) | 59.3371(0,2) | 60.7178(4,1) | 62.4338(1,2) | 73.8585(2,2) | 76.7067(5,1) | 91.7262(3,2) |
| | 0.5 | 28.3852(0,1) | 53.8662(1,1) | 62.5998(0,2) | 64.4380(2,1) | 70.7750(3,1) | 71.0430(1,2) | 78.6410(4,1) | 88.8480(5,1) | 99.7139(2,2) | 101.433(6,1) |
| | 0.9 | 11.0029(0,1) | 22.5415(1,1) | 36.2587(2,1) | 41.0682(0,2) | 51.8567(3,1) | 61.0022(1,2) | 69.0333(4,1) | 82.2210(2,2) | 86.1322(0,3) | 87.5197(5,1) |

The values in brackets $(n,s)$ denote the number of nodal diameters $(n)$ and the mode sequence $(s)$ for a given $n$ value.

Table 4
Frequency parameters $\lambda = \omega R^2\sqrt{\rho h/D}$ for circular Mindlin plates with one concentric ring support ($h/R = 0.20$)

| Edge conditions | $\frac{a_1}{R}$ | Mode sequence | | | | | | | | | |
|---|---|---|---|---|---|---|---|---|---|---|---|
| | | 1 | 2 | 3 | 4 | 5 | 6 | 7 | 8 | 9 | 10 |
| Free | 0.1 | 2.04135(1,1) | 3.65298(0,1) | 5.14059(2,1) | 11.3213(3,1) | 18.2888(0,2) | 18.8351(4,1) | 20.1456(1,2) | 27.2931(5,1) | 28.8798(2,2) | 36.4149(6,1) |
| | 0.5 | 6.59282(0,1) | 8.10007(1,1) | 9.66846(2,1) | 13,5734(3,1) | 19.8791(4,1) | 25.0294(0,2) | 27.7696(5,1) | 36.6310(6,1) | 44.5216(1,2) | 46.0945(7,1) |
| | 0.9 | 5.97155(0,1) | 15.4196(1,1) | 26.2893(2,1) | 29.4986(0,2) | 37.9670(3,1) | 43.6592(1,2) | 50.0528(4,1) | 57.6388(2,2) | 59.7240(0,3) | 62.3487(5,1) |
| Simply | 0.1 | 13.3597(0,1) | 14.4931(1,1) | 22.1178(2,1) | 32.1456(3,1) | 39.3178(0,2) | 41.5383(1,2) | 42.7947(4,1) | 50.9331(2,2) | 53.7539(5,1) | 63.2334(3,2) |
| supported | 0.5 | 23.1506(0,1) | 34.7539(1,1) | 36.3644(0,2) | 38.4842(2,1) | 43.3853(3,1) | 48.5280(1,2) | 50.0566(4,1) | 58.2618(5,1) | 67.5961(6,1) | 70.8801(2,2) |
| | 0.9 | 9.31872(0,1) | 18.7053(1,1) | 29.2641(2,1) | 32.7908(0,2) | 40.5970(3,1) | 46.8975(1,2) | 52.4147(4,1) | 61.0155(2,2) | 63.5152(0,3) | 64.5238(5,1) |
| Clamped | 0.1 | 19.0738(0,1) | 19.9633(1,1) | 27.2099(2,1) | 36.8621(3,1) | 44.3314(0,2) | 46.4687(1,2) | 47.0455(4,1) | 55.1949(2,2) | 57.5117(5,1) | 66.8114(3,2) |
| | 0.5 | 23.9924(0,1) | 42.4304(1,1) | 45.4603(0,2) | 46.9089(2,1) | 50.4382(1,2) | 50.5887(3,1) | 55.9549(4,1) | 63.0277(5,1) | 71.0501(2,2) | 71.4632(6,1) |
| | 0.9 | 9.93685(0,1) | 19.4728(1,1) | 30.0197(2,1) | 33.6358(0,2) | 41.2681(3,1) | 47.6736(1,2) | 52.9783(4,1) | 61.6767(2,2) | 64.2239(0,3) | 64.9816(5,1) |

The values in brackets $(n,s)$ denote the number of nodal diameters $(n)$ and the mode sequence $(s)$ for a given $n$ value.

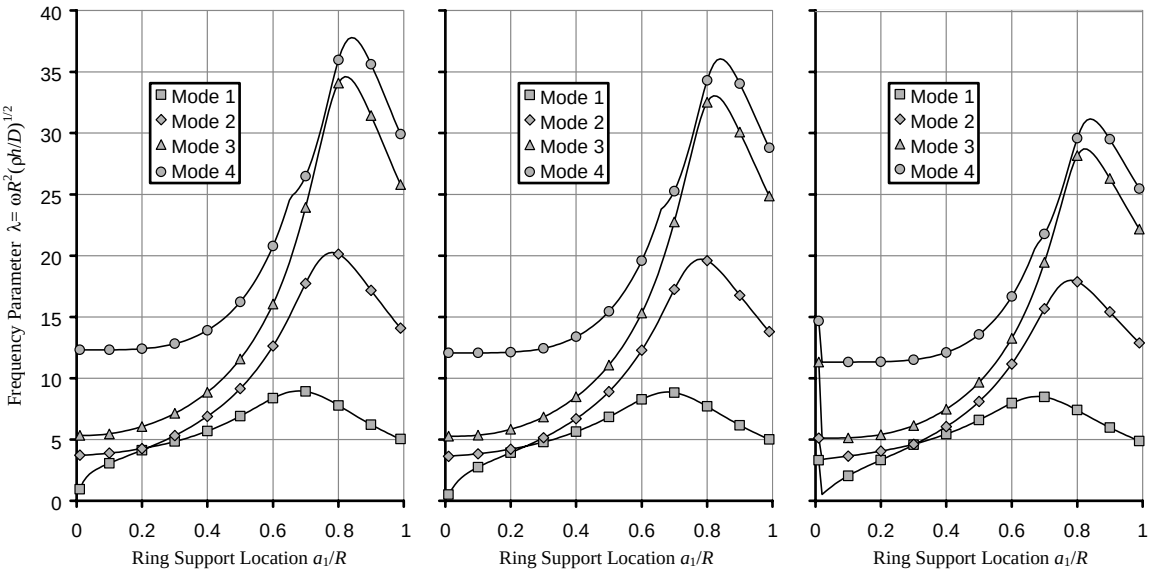


(a) Thickness Ratio $h/R = 0.05$ (b) Thickness Ratio $h/R = 0.10$ (c) Thickness Ratio $h/R = 0.20$

Fig. 2. Frequency parameters $\lambda = \omega R^2(\rho h/D)^{1/2}$ versus ring support locations $a_1/R$ for free circular Mindlin plates having one concentric ring support and plate thickness ratios $h/R = 0.05$, 0.10 and 0.20.

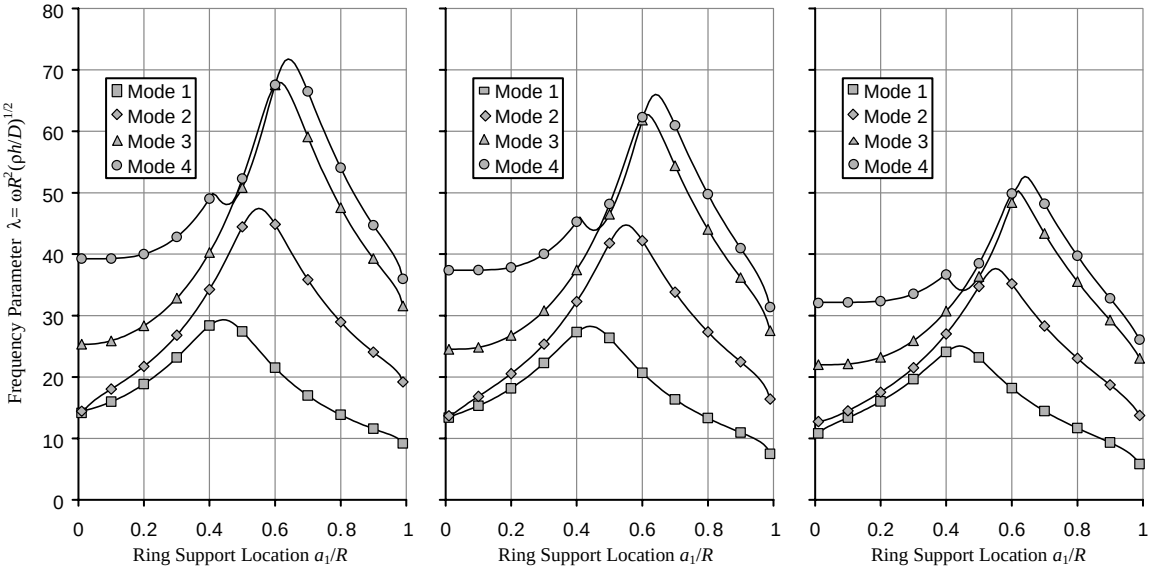


(a) Thickness Ratio $h/R = 0.05$ (b) Thickness Ratio $h/R = 0.10$ (c) Thickness Ratio $h/R = 0.20$

Fig. 3. Frequency parameters $\lambda = \omega R^2(\rho h/D)^{1/2}$ versus ring support locations $a_1/R$ for simply supported circular Mindlin plates having one concentric ring support and plate thickness ratios $h/R = 0.05$, 0.10 and 0.20.

Fig. 4 presents the relationship between the frequency parameters $\lambda$ of the first four modes and the ring support location $a_1/R$ for clamped circular Mindlin plates. The frequency parameters $\lambda$ against the ring

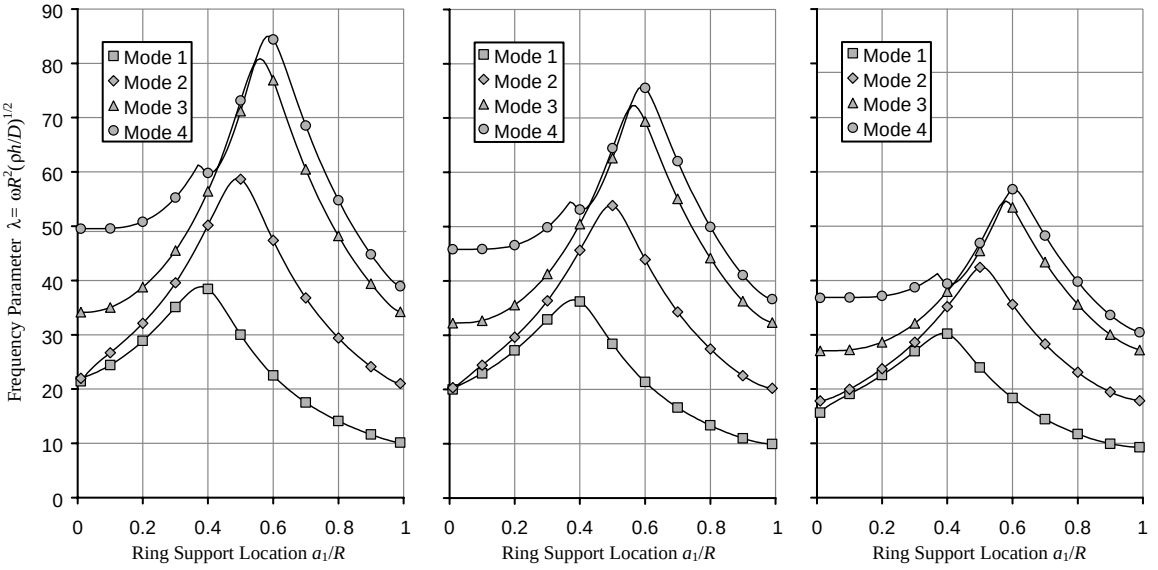


Fig. 4. Frequency parameters $\lambda = \omega R^2(\rho h/D)^{1/2}$ versus ring support locations $a_1/R$ for clamped circular Mindlin plates having one concentric ring support and plate thickness ratios $h/R = 0.05$, 0.10 and 0.20.

support location $a_1/R$ show very similar trends as in the cases for simply supported circular Mindlin plates shown in Fig. 3. However, the optimal ring support locations for the first four modes in the clamped plates are moved to $a_1/R \approx 0.38$, 0.49, 0.56 and 0.59, respectively.

Figs. 2–4 also show that the effect of transverse shear deformation and rotary inertia on the vibration frequencies is more pronounced for the circular plates with higher degree of edge constraint (in the order from free to simply supported to clamped).

The exact mode shapes of the displacement fields $\bar{w}$, $\psi_r$ and $\psi_\theta$ and the stress resultants $Q_r$, $M_{rr}$ and $M_{r\theta}$ for the first four modes in the radial direction are presented in Figs. 5–7 for free, simply supported and clamped circular Mindlin plates with one concentric ring support. The mode shapes in the circumferential direction are governed by $\cos n\theta$ for $\bar{w}$, $\psi_r$, $Q_r$ and $M_{rr}$, and by $\sin n\theta$ for $\psi_\theta$ and $M_{r\theta}$, respectively (see Appendix A), where $n$ is the number of nodal diameters of the vibrating mode. The plate thickness ratio is set to be $h/R = 0.10$ and the location of the ring support is at $a_1/R = 0.5$. All mode shapes are obtained by setting $R = 1$ and $E = 1$, and are scaled by multiplying the factor $(1/|\bar{w}_{\max}|)$.

As expected, the rotation $\psi_\theta$ and the bending moment $M_{r\theta}$ for an axisymmetric mode ($n = 0$) are equal to zero (see Figs. 5–7). The discontinuity of the shear force $Q_r$ at the location of the ring support ($a_1/R = 0.5$) occurs in all cases shown in Figs. 5–7. The bending moment $M_{rr}$ exhibits slope discontinuity at the location of the ring support. These discontinuity features may not be captured if one uses a numerical method, such as the Ritz method or the finite strip method, to study the ring supported circular plates.

### 3.3. Circular plates with two concentric ring supports

Tables 5–7 present the exact frequency parameters $\lambda$ of the first 10 modes for free, simply supported and clamped circular Mindlin plates with two concentric ring supports. The plate thickness ratios are set to be

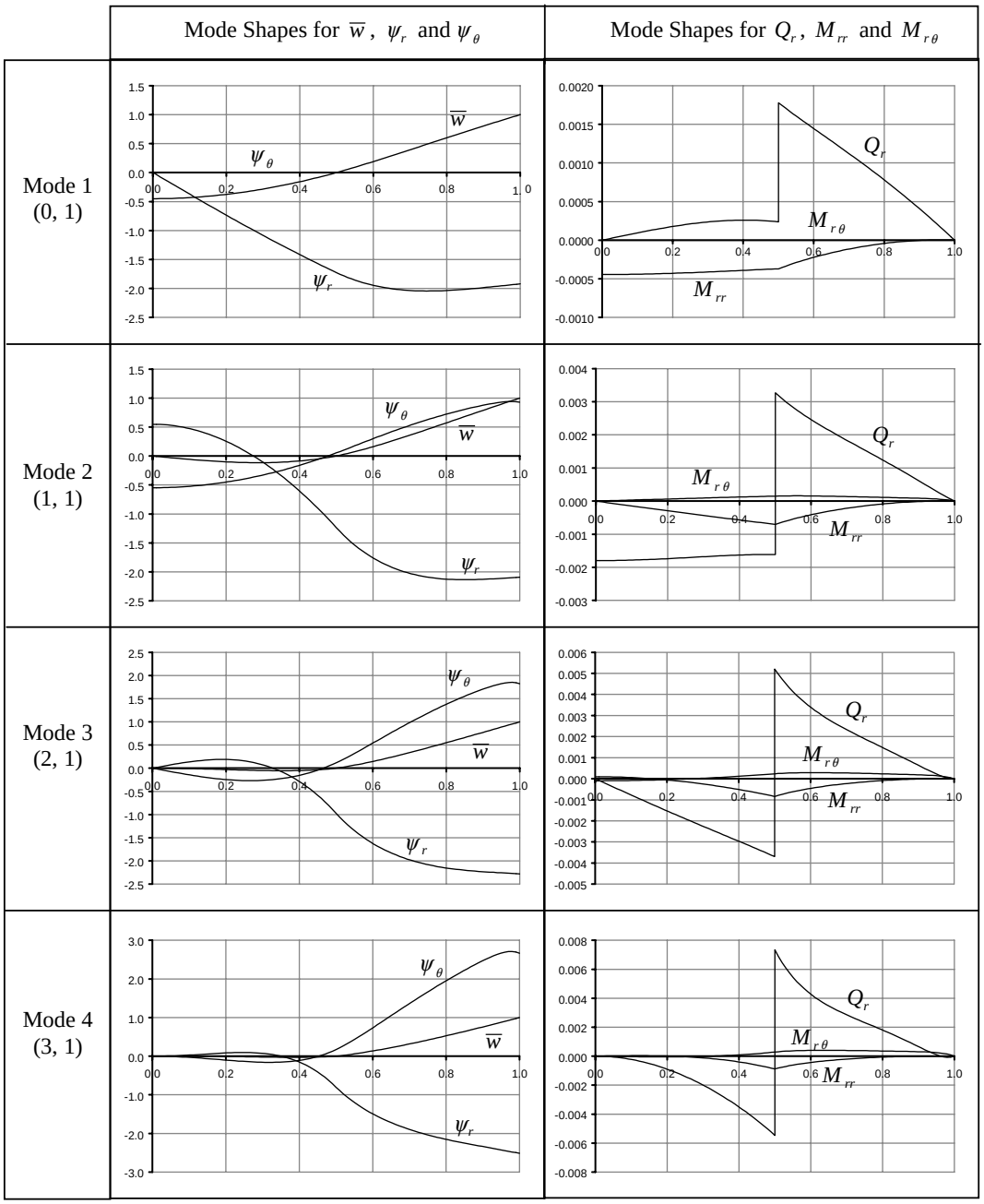


Fig. 5. The mode shapes of displacement fields and stress resultants for a free circular Mindlin plate with one concentric ring support ($h/R = 0.1$, $a_1/R = 0.5$). The values in brackets $(n, s)$ denote the number of nodal diameters $(n)$ and the mode sequence $(s)$ for a given $n$ value.

$h/R = 0.05$, 0.10 and 0.20 and the locations of the two ring supports $a_1/R$ and $a_2R$ are at 0.8 and 0.2, and 2/3 and 1/3, respectively.

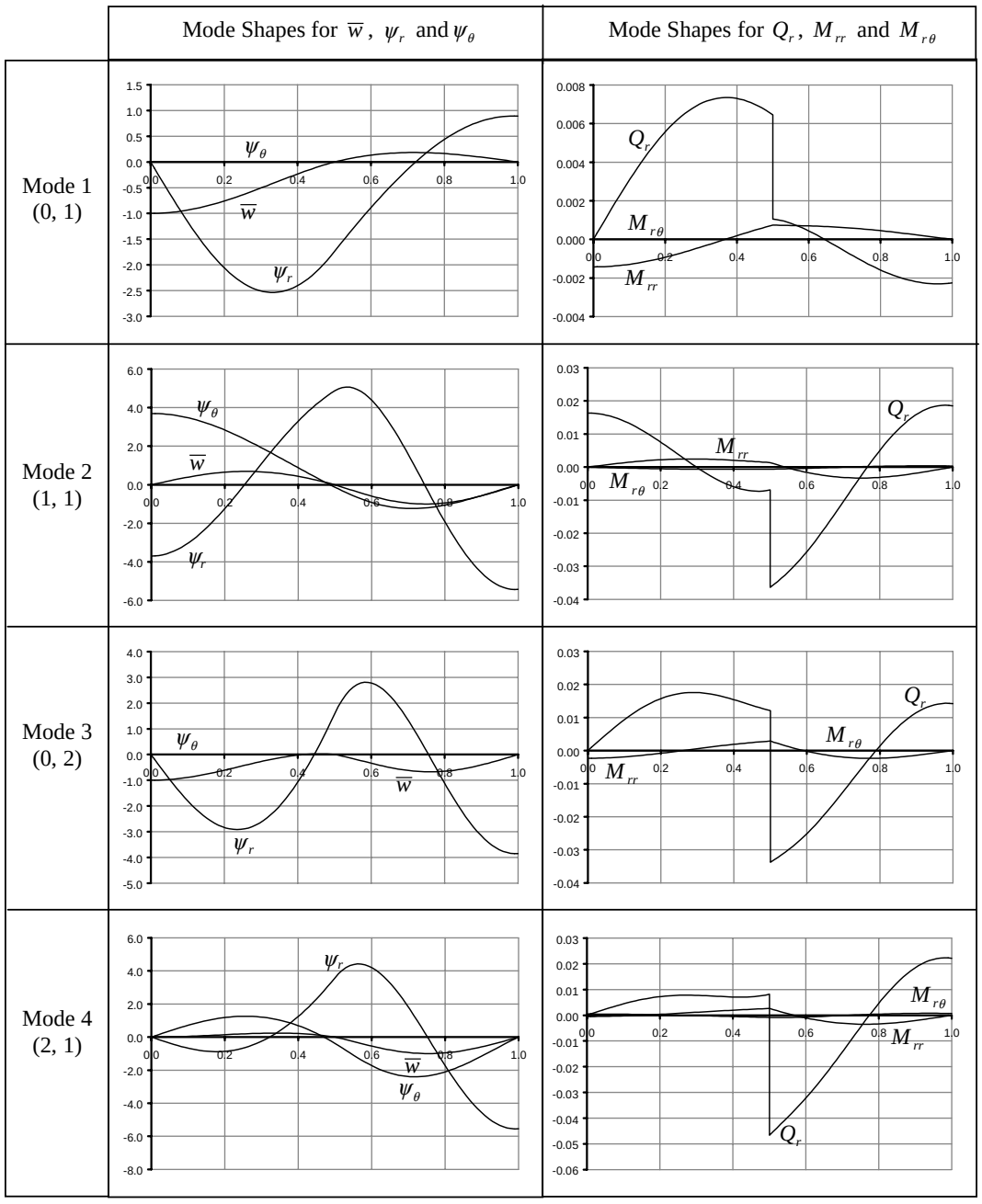


Fig. 6. The mode shapes of displacement fields and stress resultants for a simply supported circular Mindlin plate with one concentric ring support ($h/R = 0.1$, $a_1/R = 0.5$). The values in brackets $(n, s)$ denote the number of nodal diameters ($n$) and the mode sequence ($s$) for a given $n$ value.

We observe that shear deformation and rotary inertia have more significant effects on vibration of circular Mindlin plates with two ring supports than with one ring support. It is interesting to note that the

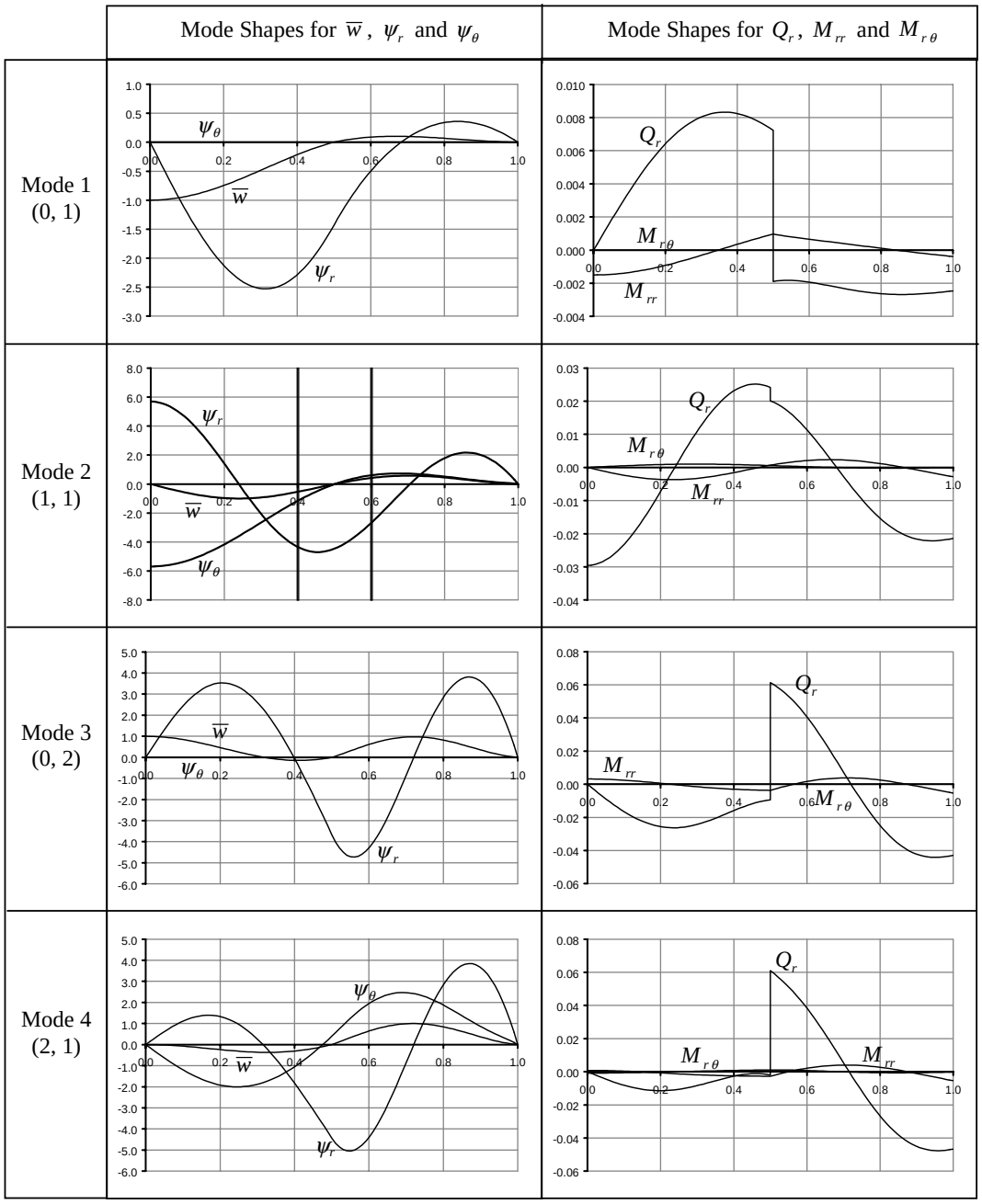


Fig. 7. The mode shapes of displacement fields and stress resultants for a clamped Mindlin plate with one concentric ring support ($h/R = 0.1$, $a_1/R = 0.5$). The values in brackets $(n, s)$ denote the number of nodal diameters $(n)$ and the mode sequence $(s)$ for a given $n$ value.

vibration patterns $(n, s)$ of the first 10 modes for circular Mindlin plates with two ring supports are changed when the plate thickness ratio $h/R$ increases from 0.05 to 0.10 to 0.20 (see Tables 5–7), whereas the patterns $(n, s)$ remain the same for circular Mindlin plates with one ring support (see Tables 2–4).

Table 5
Frequency parameters $\lambda = \omega R^2\sqrt{\rho h/D}$ for circular Mindlin plates with two concentric ring supports ($h/R = 0.05$)

| Edge conditions | $\frac{a_1}{R}$ | $\frac{a_2}{R}$ | Mode sequence | | | | | | | | | |
|---|---|---|---|---|---|---|---|---|---|---|---|---|
| | | | 1 | 2 | 3 | 4 | 5 | 6 | 7 | 8 | 9 | 10 |
| Free | 0.8 | 0.2 | 26.7387(0,1) | 30.2797(1,1) | 37.4580(2,1) | 47.7174(3,1) | 58.5918(4,1) | 59.1371(0,2) | 62.7393(1,2) | 69.1697(2,2) | 69.4588(5,1) | 81.0067(6,1) |
| | 2/3 | 1/3 | 18.9882(0,1) | 19.9908(1,1) | 22.3798(2,1) | 26.6649(3,1) | 33.2159(4,1) | 42.1541(5,1) | 53.4388(6,1) | 64.0177(0,2) | 66.9618(7,1) | 82.5920(8,1) |
| Simply | 0.8 | 0.2 | 42.8181(0,1) | 47.7876(1,1) | 56.8489(2,1) | 72.9069(3,1) | 95.4730(4,1) | 117.819(0,2) | 122.551(5,1) | 129.512(1,2) | 142.225(2,2) | 152.719(6,1) |
| supported | 2/3 | 1/3 | 62.9088(0,1) | 92.3646(1,1) | 94.6352(0,2) | 98.4527(2,1) | 106.916(3,1) | 117.342(4,1) | 126.552(1,2) | 129.511(5,1) | 141.523(0,3) | 143.374(6,1) |
| Clamped | 0.8 | 0.2 | 43.6131(0,1) | 48.6259(1,1) | 57.6841(2,1) | 73.7453(3,1) | 96.3550(4,1) | 119.510(0,2) | 123.516(5,1) | 131.611(1,2) | 144.444(2,2) | 153.803(6,1) |
| | 2/3 | 1/3 | 63.6957(0,1) | 107.905(1,1) | 117.719(0,2) | 121.987(2,1) | 134.719(3,1) | 147.664(1,2) | 149.253(4,1) | 164.111(5,1) | 164.138(0,3) | 167.176(2,2) |

The values in brackets $(n, s)$ denote the number of nodal diameters $(n)$ and the mode sequence $(s)$ for a given $n$ value.

Table 6
Frequency parameters $\lambda = \omega R^2\sqrt{\rho h/D}$ for circular Mindlin plates with two concentric ring supports ($h/R = 0.10$)

| Edge conditions | $\frac{a_1}{R}$ | $\frac{a_2}{R}$ | Mode sequence | | | | | | | | | |
|---|---|---|---|---|---|---|---|---|---|---|---|---|
| | | | 1 | 2 | 3 | 4 | 5 | 6 | 7 | 8 | 9 | 10 |
| Free | 0.8 | 0.2 | 25.5086(0,1) | 28.4228(1,1) | 35.0107(2,1) | 44.1723(3,1) | 53.0417(4,1) | 53.5368(0,2) | 55.8289(1,2) | 60.6891(2,2) | 61.5782(5,1) | 70.6965(6,1) |
| | 2/3 | 1/3 | 18.1175(0,1) | 18.8987(1,1) | 20.9497(2,1) | 24.7705(3,1) | 30.6945(4,1) | 38.7693(5,1) | 48.8445(6,1) | 57.9897(0,2) | 60.6819(7,1) | 74.0268(8,1) |
| Simply | 0.8 | 0.2 | 39.2323(0,1) | 42.8131(1,1) | 50.5876(2,1) | 64.9151(3,1) | 84.0971(4,1) | 102.241(0,2) | 105.865(5,1) | 109.276(1,2) | 118.615(2,2) | 129.061(6,1) |
| supported | 2/3 | 1/3 | 57.3773(0,1) | 81.7030(1,1) | 82.9954(0,2) | 86.8296(2,1) | 93.3530(3,1) | 101.303(4,1) | 106.294(1,2) | 110.435(5,1) | 113.600(0,3) | 116.970(2,2) |
| Clamped | 0.8 | 0.2 | 39.4396(0,1) | 43.0213(1,1) | 50.7805(3,1) | 65.0942(3,1) | 84.2705(4,1) | 102.655(0,2) | 106.039(5,1) | 109.754(1,2) | 119.754(2,2) | 129.238(6,1) |
| | 2/3 | 1/3 | 57.7223(0,1) | 93.6350(1,1) | 98.5652(0,2) | 102.718(2,1) | 111.972(3,1) | 120.153(1,2) | 122.261(4,1) | 127.036(0,3) | 129.095(2,2) | 131.623(5,1) |

The values in brackets $(n, s)$ denote the number of nodal diameters $(n)$ and the mode sequence $(s)$ for a given $n$ value.

Table 7
Frequency parameters $\lambda = \omega R^2\sqrt{\rho h/D}$ for circular Mindlin plates with two concentric ring supports ($h/R = 0.20$)

| Edge conditions | $\frac{a_1}{R}$ | $\frac{a_2}{R}$ | Mode sequence | | | | | | | | | |
|---|---|---|---|---|---|---|---|---|---|---|---|---|
| | | | 1 | 2 | 3 | 4 | 5 | 6 | 7 | 8 | 9 | 10 |
| Free | 0.8 | 0.2 | 21.9332(0,1) | 23.8245(1,1) | 29.3685(2,1) | 35.7033(3,1) | 40.8967(4,1) | 41.0367(0,2) | 41.6505(1,2) | 44.4982(2,2) | 46.1839(5,1) | 51.9438(3,2) |
| | 2/3 | 1/3 | 15.6243(0,1) | 16.0256(1,1) | 17.4400(2,1) | 20.4062(3,1) | 25.2120(4,1) | 31.6859(5,1) | 39.4332(6,1) | 44.7877(0,2) | 48.0773(7,1) | 57.3345(8,1) |
| Simply | 0.8 | 0.2 | 30.7545(0,1) | 32.4324(1,1) | 38.6921(2,1) | 49.5617(3,1) | 62.5962(4,1) | 73.4010(0,2) | 75.8496(1,2) | 76.3557(5,1) | 82.0522(2,2) | 90.3321(6,1) |
| supported | 2/3 | 1/3 | 44.7146(0,1) | 61.3554(0,2) | 61.8197(1,1) | 64.5555(2,1) | 68.3117(3,1) | 71.8781(1,2) | 72.8621(4,1) | 73.0000(0,3) | 75.6072(2,2) | 78.3257(5,1) |
| Clamped | 0.8 | 0.2 | 30.8371(0,1) | 32.5085(1,1) | 38.7525(2,1) | 49.6072(3,1) | 62.6302(4,1) | 73.4505(0,2) | 75.8967(1,2) | 76.3805(5,1) | 82.0901(2,2) | 90.3499(6,1) |
| | 2/3 | 1/3 | 44.7276(0,1) | 66.9038(1,1) | 67.2324(0,2) | 71.0512(2,1) | 76.3436(3,1) | 78.0453(1,2) | 78.9163(0,3) | 79.7483(2,2) | 80.7312(4,1) | 83.3910(3,2) |

The values in brackets $(n,s)$ denote the number of nodal diameters $(n)$ and the mode sequence $(s)$ for a given $n$ value.

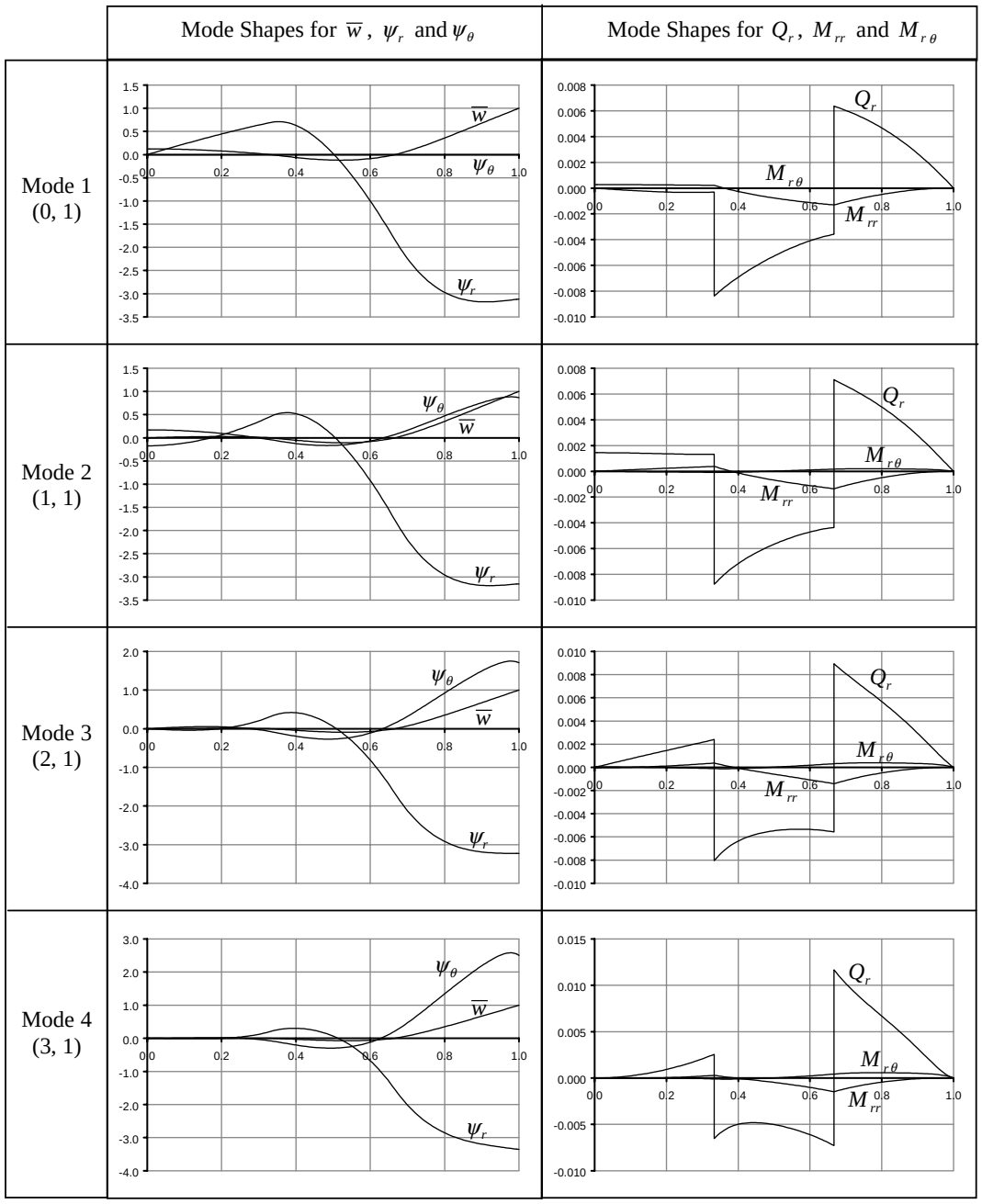


Fig. 8. The mode shapes of displacement fields and stress resultants for a free Mindlin plate with two concentric ring supports ($h/R = 0.1$, $a_1/R = 2/3$ and $a_2/R = 1/3$). The values in brackets $(n, s)$ denote the number of nodal diameters ($n$) and the mode sequence ($s$) for a given $n$ value.

The mode shapes of the displacement fields $\bar{w}$, $\psi_r$ and $\psi_\theta$ and the stress resultants $Q_r$, $M_{rr}$ and $M_{r\theta}$ for the first four modes in the radial direction are presented in Fig. 8 for a free circular Mindlin plate with two

Table 8
Frequency parameters $\lambda = \omega R^2\sqrt{\rho h/D}$ for circular Mindlin plates with three concentric ring supports ($a_1/R = 0.75$, $a_2/R = 0.5$ and $a_3/R = 0.25$)

| Edge conditions | $\frac{h}{R}$ | Mode sequence | | | | | | | | | |
|---|---|---|---|---|---|---|---|---|---|---|---|
| | | 1 | 2 | 3 | 4 | 5 | 6 | 7 | 8 | 9 | 10 |
| Free | 0.05 | 34.2426(0,1) | 35.0327(1,1) | 37.3961(2,1) | 41.5248(3,1) | 47.6238(4,1) | 55.8321(5,1) | 66.1962(6,1) | 78.6875(7,1) | 93.2325(8,1) | 109.737(9,1) |
| | 0.10 | 31.4283(0,1) | 32.0499(1,1) | 33.9871(2,1) | 37.4574(3,1) | 42.6801(4,1) | 49.7687(5,1) | 58.6993(6,1) | 69.3467(7,1) | 81.5337(8,1) | 94.4572(0,2) |
| | 0.20 | 25.0424(0,1) | 25.4020(1,1) | 26.6331(2,1) | 29.0751(3,1) | 32.9909(4,1) | 38.3926(5,1) | 45.0802(6,1) | 52.7771(7,1) | 61.2250(8,1) | 67.3413(0,2) |
| Simply supported | 0.05 | 109.509(0,1) | 153.369(1,1) | 154.521(0,2) | 159.790(2,1) | 167.929(3,1) | 177.942(4,1) | 189.644(5,1) | 189.923(1,2) | 201.441(0,3) | 202.945(6,1) |
| | 0.10 | 94.4059(0,1) | 129.922(0,2) | 130.244(1,1) | 134.455(2,1) | 140.116(3,1) | 147.038(4,1) | 151.169(1,2) | 154.771(0,3) | 155.094(5,1) | 160.440(2,2) |
| | 0.20 | 67.3413(0,1) | 90.9059(0,2) | 91.6098(1,1) | 93.5827(2,1) | 96.3068(0,3) | 96.3800(3,1) | 96.9311(1,2) | 99.9097(4,1) | 101.028(2,2) | 104.116(5,1) |
| Clamped | 0.05 | 109.667(0,1) | 170.028(1,1) | 176.318(0,2) | 182.895(2,1) | 196.039(3,1) | 210.89(4,1) | 214.418(1,2) | 226.909(5,1) | 229.899(0,3) | 235.651(2,2) |
| | 0.10 | 94.4278(0,1) | 140.047(1,1) | 141.516(0,2) | 147.625(2,1) | 156.390(3,1) | 165.116(1,2) | 165.978(4,1) | 170.147(0,3) | 174.762(2,2) | 176.218(5,1) |
| | 0.20 | 67.3413(0,1) | 93.4092(0,2) | 94.3554(1,1) | 97.7473(2,1) | 101.166(1,2) | 101.283(0,3) | 101.776(3,1) | 105.435(2,2) | 106.427(4,1) | 109.685(3,2) |

The values in brackets $(n, s)$ denote the number of nodal diameters $(n)$ and the mode sequence $(s)$ for a given $n$ value.

concentric ring supports ($h/R = 0.10$, $a_1/R = 2/3$ and $a_2/R = 1/3$). Again, the discontinuities in stress resultants $Q_r$ and $M_{rr}$ due to the presence of the ring supports are observed.

### 3.4. Circular plates with three concentric ring supports

Table 8 presents the exact frequency parameters $\lambda$ of the first 10 modes for free, simply supported and clamped circular Mindlin plates with three concentric ring supports. The plate thickness ratios are set to be $h/R = 0.05$, 0.10 and 0.20 and the locations of the three ring supports $a_1/R, a_2/R$ and $a_3/R$ are at 0.75, 0.50 and 0.25, respectively.

The effect of transverse shear deformation and rotary inertia is more pronounced for plates with three ring supports (see Table 8). For example, when the plate thickness ratio $h/R$ varies from 0.05 to 0.2, the fundamental frequency parameter $\lambda$ of a free circular plate decreases by 4.54% for the plate with one ring support ($a_1/R = 0.5$), 17.72% with two ring supports ($a_1/R = 2/3$ and $a_2/R = 1/3$), and 26.87% with three ring supports ($a_1/R = 0.75$, $a_2/R = 0.50$ and $a_3/R = 0.25$), respectively. The vibration patterns $(n, s)$ of the first 10 modes for circular Mindlin plates with three ring supports are changed when the plate thickness ratio $h/R$ increases from 0.05 to 0.10 to 0.20 (see Table 8).

## 4. Conclusions

This paper presents an analytical approach to investigate the vibration behaviour of circular Mindlin plates with multiple concentric ring supports. A circular plate with ring supports is divided into several annular segments and one circular segment at the locations of the ring supports and the domain decomposition technique is utilized to develop the analytical method.

The vibration behaviour of circular Mindlin plates with one, two and three concentric ring supports is studied. Several conclusions may be drawn from this study:

(1) The effect of transverse shear deformation and rotary inertia on the vibration of a circular plate is more pronounced when the plate thickness ratio $h/R$ is large, or the plate has a higher degree of edge constraints (in the order from free, to simply supported to clamped), or the plate has more concentric ring supports.
(2) For circular plates with one concentric ring support, the optimal location of the ring support for the first four modes is in the range $a_1/R \approx 0.70$ to 0.85 for free plates, $a_1/R \approx 0.45$ to 0.65 for simply supported plates, and $a_1/R \approx 0.38$ to 0.59 for clamped plates, respectively. The optimal locations of the ring support for higher modes are closer to the edge of the plate; and
(3) the discontinuity of the shear force $Q_r$ at the locations of the ring supports exists for all considered cases. The discontinuity of the slope of the bending moment $M_{rr}$ at the locations of the ring supports also exists for all considered cases. These discontinuity features may not be correctly captured if one uses the numerical method, such as the p-Ritz method or the finite strip method, to study such plates.

The proposed method is able to obtain exact vibration solutions for circular Mindlin plates with arbitrary number of concentric ring supports. This method can also be modified to study circular and annular Mindlin plates with stepped thickness variations and concentric elastic ring supports. Further research in these directions will be carried out and the research findings will be reported in future publications.

**Acknowledgements**

The work described in this paper was fully supported by a research grant from the University of Western Sydney (grand no. 20801-80355). The first author would like to thank Ms L. Zhou for preparing the graphs and tables in this paper.

## Appendix A. Displacement fields and stress resultants

The displacement fields and the stress resultants of the $i$th segment in a ring supported circular plate may be expressed as

$$\bar{w}^i = [A_1^i R_n^i(\Delta_1\chi) + A_2^i R_n^i(\Delta_2\chi) + B_1^i S_n^i(\Delta_1\chi) + B_2^i S_n^i(\Delta_2\chi)]\cos n\theta \tag{A.1}$$

$$\psi_r^i = \left[A_1^i(\sigma_1-1)R_n^{i'}(\Delta_1\chi) + A_2^i(\sigma_2-1)R_n^{i'}(\Delta_2\chi) + A_3^i\frac{n}{\chi}R_n^i(\Delta_3\chi) + B_1^i(\sigma_1-1)S_n^{i'}(\Delta_1\chi) + B_2^i(\sigma_2-1)S_n^{i'}(\Delta_2\chi) + B_3^i\frac{n}{\chi}S_n^i(\Delta_3\chi)\right]\cos n\theta \tag{A.2}$$

$$\psi_\theta^i = \left[-A_1^i\frac{n(\sigma_1-1)}{\chi}R_n^i(\Delta_1\chi) - A_2^i\frac{n(\sigma_2-1)}{\chi}R_n^i(\Delta_2\chi) - A_3^iR_n^{i'}(\Delta_3\chi) - B_1^i\frac{n(\sigma_1-1)}{\chi}S_n^i(\Delta_1\chi) - B_2^i\frac{n(\sigma_2-1)}{\chi}S_n^i(\Delta_2\chi) - B_3^iS_n^{i'}(\Delta_3\chi)\right]\sin n\theta \tag{A.3}$$

$$Q_r^i = \kappa^2 Gh\left[A_1^i\sigma_1R_n^{i'}(\Delta_1\chi) + A_2^i\sigma_2R_n^{i'}(\Delta_2\chi) + A_3^i\frac{n}{\chi}R_n^i(\Delta_3\chi) + B_1^i\sigma_1S_n^{i'}(\Delta_1\chi) + B_2^i\sigma_2S_n^{i'}(\Delta_2\chi) + B_3^i\frac{n}{\chi}S_n^i(\Delta_3\chi)\right]\times\cos n\theta \tag{A.4}$$

$$\begin{aligned}M_{rr}^i = \frac{D}{R}\Bigg\{&A_1^i\left[(\sigma_1-1)R_n^{i''}(\Delta_1\chi) + \frac{v}{\chi}(\sigma_1-1)R_n^{i'}(\Delta_1\chi) - \frac{v}{\chi^2}n^2(\sigma_1-1)R_n^i(\Delta_1\chi)\right]\\ &+A_2^i\left[(\sigma_2-1)R_n^{i''}(\Delta_2\chi) + \frac{v}{\chi}(\sigma_2-1)R_n^{i'}(\Delta_2\chi) - \frac{v}{\chi^2}n^2(\sigma_2-1)R_n^i(\Delta_2\chi)\right]\\ &+A_3^i\left[\frac{n}{\chi}R_n^{i'}(\Delta_3\chi) - \frac{n}{\chi^2}R_n^i(\Delta_3\chi) + \frac{vn}{\chi^2}R_n^i(\Delta_3\chi) - \frac{vn}{\chi}R_n^{i'}(\Delta_3\chi)\right]\\ &+B_1^i\left[(\sigma_1-1)S_n^{i''}(\Delta_1\chi) + \frac{v}{\chi}(\sigma_1-1)S_n^{i'}(\Delta_1\chi) - \frac{v}{\chi^2}n^2(\sigma_1-1)S_n^i(\Delta_1\chi)\right]\\ &+B_2^i\left[(\sigma_2-1)S_n^{i''}(\Delta_2\chi) + \frac{v}{\chi}(\sigma_2-1)S_n^{i'}(\Delta_2\chi) - \frac{v}{\chi^2}n^2(\sigma_2-1)S_n^i(\Delta_2\chi)\right]\\ &+B_3^i\left[\frac{n}{\chi}S_n^{i'}(\Delta_3\chi) - \frac{n}{\chi^2}S_n^i(\Delta_3\chi) + \frac{vn}{\chi^2}S_n^i(\Delta_3\chi) - \frac{vn}{\chi}S_n^{i'}(\Delta_3\chi)\right]\Bigg\}\cos n\theta\end{aligned} \tag{A.5}$$

$$
\begin{aligned}
M^i_{r\theta} = \frac{D}{R}\left(\frac{1-v}{2}\right)\Bigg\{ & A^i_1\Bigg[-\frac{n(\sigma_1-1)}{\chi}R^{i'}_n(\Delta_1\chi)+\frac{n(\sigma_1-1)}{\chi^2}R^i_n(\Delta_1\chi)-\frac{n(\sigma_1-1)}{\chi}R^{i'}_n(\Delta_1\chi) \\
& +\frac{n(\sigma_1-1)}{\chi^2}R^i_n(\Delta_1\chi)\Bigg]+A^i_2\Bigg[-\frac{n(\sigma_2-1)}{\chi}R^{i'}_n(\Delta_2\chi)+\frac{n(\sigma_2-1)}{\chi^2}R^i_n(\Delta_2\chi) \\
& -\frac{n(\sigma_2-1)}{\chi}R^{i'}_n(\Delta_2\chi)+\frac{n(\sigma_2-1)}{\chi^2}R^i_n(\Delta_2\chi)\Bigg]+A^i_3\Bigg[-\frac{n^2}{\chi^2}R^i_n(\Delta_3\chi)+\frac{1}{\chi}R^{i'}_n(\Delta_3\chi)-R^{i''}_n(\Delta_3\chi)\Bigg] \\
& +B^i_1\Bigg[-\frac{n(\sigma_1-1)}{\chi}S^{i'}_n(\Delta_1\chi)+\frac{n(\sigma_1-1)}{\chi^2}S^i_n(\Delta_1\chi)-\frac{n(\sigma_1-1)}{\chi}S^{i'}_n(\Delta_1\chi)+\frac{n(\sigma_1-1)}{\chi^2}S^i_n(\Delta_1\chi)\Bigg] \\
& +B^i_2\Bigg[-\frac{n(\sigma_2-1)}{\chi}S^{i'}_n(\Delta_2\chi)+\frac{n(\sigma_2-1)}{\chi^2}S^i_n(\Delta_2\chi)-\frac{n(\sigma_2-1)}{\chi}S^{i'}_n(\Delta_2\chi)+\frac{n(\sigma_2-1)}{\chi^2}S^i_n(\Delta_2\chi)\Bigg] \\
& +B^i_3\Bigg[-\frac{n^2}{\chi^2}S^i_n(\Delta_3\chi)+\frac{1}{\chi}S^{i'}_n(\Delta_3\chi)-S^{i''}_n(\Delta_3\chi)\Bigg]\Bigg\}\sin n\theta
\end{aligned}
\tag{A.6}
$$

where the primes ($'$) and ($''$) denote the first and second derivatives with respect to $\chi$, respectively.

## References


Aksu, G., Al-Kaabi, S.A., 1987. Free vibration analysis of Mindlin plates with linearly varying thickness. Journal of Sound and Vibration 119, 189–205.

Bodine, R.Y., 1959. The fundamental frequency of a thin, flat, circular plate simply supported along a circle of arbitrary radius. Transactions of ASME Journal of Applied Mechanics 26, 666–668.

Chakraverty, S., Petyt, M., 1999. Free vibration analysis of elliptic and circular plates having rectangular orthotropy. Structural Engineering and Mechanics 7 (1), 53–67.

Chou, F.S., Wang, C.M., Cheng, G.D., Olhoff, N., 1999. Optimal design of internal ring supports for vibrating circular plates. Journal of Sound and Vibration 219 (3), 525–537.

Gupta, U.S., Lal, R., 1985. Axisymmetric vibrations of polar orthotropic Mindlin annular plates of variable thickness. Journal of Sound and Vibration 98, 565–573.

Elishakoff, I., 2000. Axisymmetric vibration of inhomogeneous free circular plates: An unusual exact, closed-form solution. Journal of Sound and Vibration 234 (1), 167–170.

Irie, T., Yamada, G., Takagi, K., 1982. Natural frequencies of thick annular plates. Transactions of the ASME, Journal of Applied Mechanics 49, 633–638.

Kim, C.S., Dickinson, S.M., 1989. On the lateral vibration of thin annular and circular composite plates subject to certain complicating effects. Journal of Sound and Vibration 130, 363–377.

Kunukkasseril, V.X., Swamidas, A.S.J., 1974. Vibration of continuous circular plates. International Journal of Solids and Structures 10, 603–619.

Lam, K.Y., Liew, K.M., 1992. A numerical model based on orthogonal plate functions for vibration of ring supported elliptical plates. Computational Mechanics 9, 113–126.

Laura, P.A.A., 1999. Comments on "Optimal support position for a structure to maximize its fundamental natural frequency". Journal of Sound and Vibration 222, 853–856.

Laura, P.A.A., Gutierrez, R.H., Cortinez, V.H., Utjes, J.C., 1987. Transverse vibrations of circular plates and membranes with intermediate supports. Journal of Sound and Vibration 113, 81–86.

Laura, P.A.A., Sonzogni, V., Romanelli, E., 1996. Effect of Poisson's ratio on the fundamental frequency of transverse vibration and buckling load of circular plates with variable profile. Applied Acoustics 47 (3), 263–273.

Levinson, M., 1980. An accurate simple theory of the statics and dynamics of elastic plates. Mechanics Research Communications 7, 343–350.

Leissa, A.W., 1969. Vibration of plates. NASA SP-169, Office of Technology Utilization, Washington.

Leissa, A.W., 1977a. Recent research in plate vibrations: Classical theory. Shock and Vibration Digest 9, 13–24.

Leissa, A.W., 1977b. Recent research in plate vibrations: Complicating effects. Shock and Vibration Digest 9, 21–35.

Leissa, A.W., 1981a. Plate vibration research, 1976–1980: Classical theory. Shock and Vibration Digest 13, 11–22.

Leissa, A.W., 1981b. Plate vibration research, 1976–1980: Complicating effects. Shock and Vibration Digest 13, 19–36.

Leissa, A.W., 1987a. Recent research in plate vibrations, 1981–1985. Part I. Classical theory. Shock and Vibration Digest 19, 11–18.

Leissa, A.W., 1987b. Recent research in plate vibrations, 1981–1985. Part II. Complicating effects. Shock and Vibration Digest 19, 10–24.

Leung, A.Y.T., 1991. An unconstrained third-order plate theory. Computers and Structures 40 (4), 871–875.

Liew, K.M., 1994. Vibration of clamped circular symmetric laminates. Transactions of the ASME, Journal of Vibration and Acoustics 116 (2), 141–145.

Liew, K.M., Lam, K.Y., 1993. Transverse vibration of solid circular plates continuous over multiple concentric annular supports. Transactions of ASME, Journal of Applied Mechanics 60, 208–210.

Liew, K.M., Xiang, Y., Wang, C.M., Kitipornchai, S., 1993. Flexural vibration of shear deformable circular and annular plates on ring supports. Computer Methods in Applied Mechanics and Engineering 110, 301–315.

Liew, K.M., Xiang, Y., Kitipornchai, S., Wang, C.M., 1994. Buckling and vibration of annular Mindlin plates with internal concentric ring supports subject to in-plane radial pressure. Journal of Sound and Vibration 177 (5), 689–707.

Liew, K.M., Xiang, Y., Kitipornchai, S., 1995. Research on thick plate vibration: a literature survey. Journal of Sound and Vibration 180, 163–176.

Liew, K.M., Han, J.B., Xiao, Z.M., 1997. Vibration analysis of circular Mindlin plates using the differential quadrature method. Journal of Sound and Vibration 205 (5), 617–630.

Liew, K.M., Xiang, Y., Wang, C.M., Kitipornchai, S., 1998. Vibration of Mindlin Plates-Programming the p-Version Ritz Method. Elsevier Science, Oxford, UK.

Liew, K.M., Yang, B., 1999. Three-dimensional elasticity solutions for free vibrations of circular plates: a polynomials—Ritz analysis. Computer Methods in Applied Mechanics and Engineering 175 (1–2), 189–201.

Liew, K.M., Yang, B., 2000. Elasticity solutions for free vibrations of annular plates from three-dimensional analysis. International Journal of Solids and Structures 37, 7689–7702.

McGee, O.G., Leissa, A.W., Huang, C.S., Kim, J.W., 1995. Vibrations of circular plates with clamped v-notches or rigidly constrained radial cracks. Journal of Sound and Vibration 181 (2), 185–201.

Mindlin, R.D., 1951. Influence of rotatory inertia and shear on flexural motions of isotropic, elastic plates. Transactions of the ASME, Journal of Applied Mechanics 18, 31–38.

Mindlin, R.D., Deresiewicz, H., 1954. Thickness-shear and flexural vibrations of a circular disk. Journal of Applied Physics 25, 1329–1332.

Narita, Y., 1983. Free vibration of continuous polar orthotropic annular and circular plates. Journal of Sound and Vibration 93, 503–511.

Rao, S.S., Prasad, A.S., 1980. Natural frequencies of Mindlin circular plates. Transactions of the ASME, Journal of Applied Mechanics 47, 652–655.

Reddy, J.N., 1984. A simply higher-order theory for laminated composite plates. Transactions of ASME Journal of Applied Mechanics 51, 745–752.

Reissner, E., 1945. The effect of transverse shear deformation on the bending of elastic plate. Transactions of ASME Journal of Applied Mechanics 12, 69–76.

Singh, A.V., Mirza, S., 1976. Free axisymmetric vibration of a circular plate elastically supported along two concentric circles. Journal of Sound and Vibration 48, 425–429.

Wang, C.M., Thevendran, V., 1993. Vibration analysis of annular plates with concentric supports using a variant of Rayleigh–Ritz method. Journal Sound and Vibration 163, 137–149.

Wang, C.Y., 2001. On the fundamental frequency of a circular plate supported on a ring. Journal of Sound and Vibration 243 (5), 945–946.

Wu, T.Y., Liu, G.R., 2001. Free vibration analysis of circular plates with variable thickness by the generalized differential quadrature rule. International Journal of Solids and Structures 38 (44–45), 7967–7980.